Available online at www.sciencedirect.com
ScienceDirect
Journal of Nuclear Materials 362 (2007) 46–52
journal of nuclear materials
www.elsevier.com/locate/jnucmat

Phase diagram of the UO_2–FeO_{1+x} system

S.V. Bechta [a], E.V. Krushinov [a], V.I. Almjashev [b], S.A. Vitol [a], L.P. Mezentseva [b,*], Yu.B. Petrov [c,✠], D.B. Lopukh [c], V.B. Khabensky [a], M. Barrachin [d], S. Hellmann [e], K. Froment [f], M. Fisher [e], W. Tromm [g], D. Bottomley [h], F. Defoort [f], V.V. Gusarov [b]

[a] *A.P. Aleksandrov Research Institute of Technology, Sosnovy Bor, 188540, Russian Federation*
[b] *Institute of Silicate Chemistry of Russian Academy of Sciences, Nab. Makarova, 2, Saint-Petersburg 199034, Russian Federation*
[c] *Saint-Petersburg Electrotechnical University 'LETI', Prof. Popova str., 5, Saint-Petersburg 197376, Russian Federation*
[d] *Institut de Radioprotection et Sûreté Nucléaire (IRSN), BP 3 F-13115 St-Paul-Lez- Durance, France*
[e] *AREVA NP GmbH, Freyeslebenstr. 1, 91058 Erlangen, Germany*
[f] *Laboratoire de Physico-chimie et Thermohydraulique Multiphasiques (LPTM), CEA/Grenoble, DTN/SE2T/LPTM, 17 Rue des Martyrs, 38 054 Grenoble cedex 9, France*
[g] *Forschungszentrum Karlsruhe, IKET, P.O. Box 3640, 76021 Karlsruhe, Germany*
[h] *EC, Joint Research Centre, Institute for Transuranium Elements, Postfach 2340, Hermann-von-Helmholtz-Pl. 1, 76125 Karlsruhe, Germany*

Received 9 November 2005; accepted 16 November 2006

Abstract

Phase-relation studies of the UO_2–FeO_{1+x} system in an inert atmosphere are presented. The eutectic point has been determined, which corresponds to a temperature of (1335 ± 5) °C and a UO_2 concentration of (4.0 ± 0.1) mol.%. The maximum solubility of FeO in UO_2 at the eutectic temperature has been estimated as (17.0 ± 1.0) mol.%. Liquidus temperatures for a wide concentration range have been determined and a phase diagram of the system has been constructed.

1. Introduction

The conventional fuel used in modern nuclear power plants, e.g., PWR and BWR reactors, is based on UO_2, therefore the behaviour of the UO_2–metal oxide systems is the object of extensive studies (see the comprehensive inventory presented in [1]). The knowledge of the UO_2–FeO_{1+x} system is essential for the analysis of physicochemical phenomena taking place at a severe accident involving the core meltdown and, in particular, for the ex-vessel stage of accident progression, because iron oxides are present in the sacrificial materials used in core catchers [2–5].

However the published data of the UO_2–FeO_{1+x} system are quite limited. The predicted phase diagrams of related systems are presented in [6] and in Fig. 1 (dashed lines). A phase diagram of the

* Corresponding author. Present address: ul. Karbysheva, d. 10, kv. 108, Saint-Petersburg 194021, Russian Federation. Tel.: +7 812 328 85 91; fax: +7 812 328 85 89.
E-mail address: la_mez@mail.ru (L.P. Mezentseva).
✠ Deceased.

0022-3115/$ - see front matter © 2006 Elsevier B.V. All rights reserved.
doi:10.1016/j.jnucmat.2006.11.004

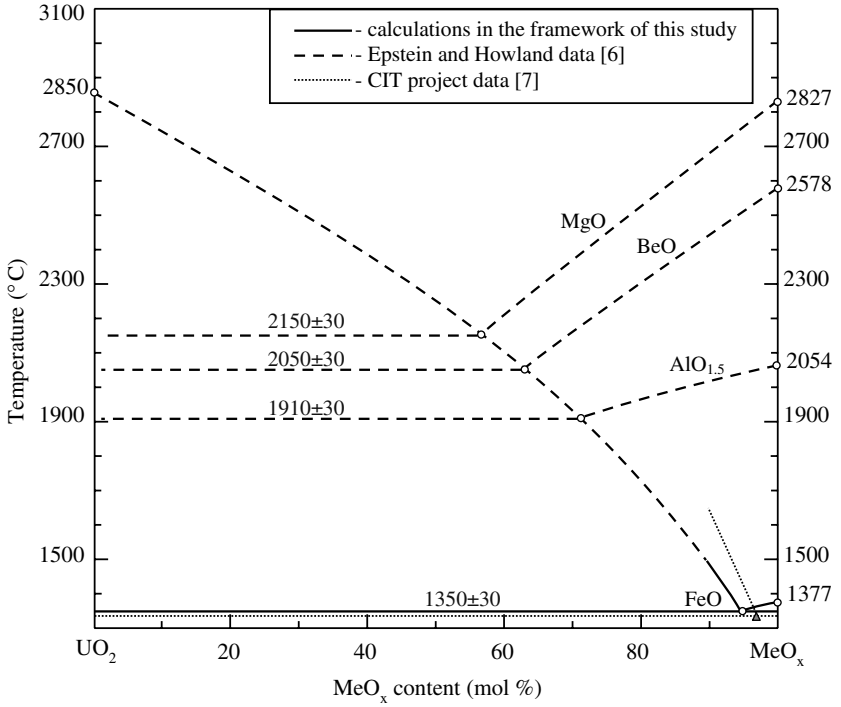

Fig. 1. Predicted UO_2–FeO phase diagram (calculated and experimental data). Dashed line – data of Ref. [6]; solid line – calculations made by the authors; dotted line – experimental data of Ref. [7].

UO_2–FeO_{1+x} system calculated by the authors using the model proposed in [6] is shown as the solid line in Fig. 1. This model was based on the ideal solution model. In accordance with these calculations the eutectic point corresponds to the temperature of ≈1350 °C and a UO_2 concentration of ≈5 mol.%.

Phase equilibria in this system have also been experimentally studied in [7]. In this work the eutectic and liquidus temperatures have been evaluated only in the concentration range of 3–10 mol.% UO_2. A eutectic point has been determined, which corresponds to 3.3 mol.% UO_2 and 1340 °C. The experimental data there and the calculated values from [6] converge well near the eutectic point, but diverge substantially at higher temperatures (Fig. 1).

The data of Voronov et al. [8] on the phase equilibria in the U–Fe–O system have been taken into account; these data were obtained by the thermobalance method followed by construction of isobaric ternary diagrams. However in this study, the oxygen partial pressure was from 580 to 21 000 Pa, and thus corresponds to the pseudo-binary sections of the U_3O_8–Fe_2O_3 and UO_2–Fe_3O_4 systems.

More detailed experimental data on the UO_2–FeO_{1+x} phase diagram are not available in the literature. This can probably be explained by the methodological difficulties, which complicate the study of this system, e.g., maintenance of the oxygen partial pressure, reactions with crucible materials, and fundamental difficulties due to a broad homogeneity range of FeO_{1+x}.

As it has already been mentioned, this is one of the basic systems used for the analysis of high-temperature physicochemical phenomena taking place in nuclear reactors and core catchers in case of a severe accident. But the divergence of modelling and experimental data of the UO_2–FeO_{1+x} phase diagram, particularly the lack of high-temperature data emphasizes the requirement for a systematic experimental study of this system.

This paper is a follow-up publication [9], which reported the ZrO_2–FeO studies within the ISTC CORPHAD Project.

2. Materials and methods

The specimens were prepared from pure UO_2 (>99.0 mass% purity; Fe; As; CuO; phosphates; chlorides not more than 0.07 mass%); FeO (not less than 99.0 mass%, impurities insoluble in HCl, sul-

phates, chlorides not more than 0.8 mass %) and Fe (>99.9 mass% purity).

The original experimental facilities and methodologies are described in detail in [9].

Specimens for studying the UO_2–FeO_{1+x} system were produced by the method of induction melting in a cold crucible (IMCC) at the RASPLAV-2 and RASPLAV-3 test facilities in flowing argon. In order to crystallize iron oxide as a wüstite structure ($Fe_{1-x}O$) with a certain composition that would be the closest to the FeO stoichiometry ($Fe_{0.946}O$ or $FeO_{1.057}$) [10], pure metallic iron (Fe > 99.9 mass% purity) was added to the initial mass as a getter in the quantity of 1 mass% in excess of the total mass (as was done with the ZrO_2–FeO system investigation [9]).

The phase composition (phase identification) of the specimens was determined by X-ray diffraction analysis using the X-ray diffractometer DRON-3 based in this case on FeK_α radiation ($\lambda = 193.73$ pm).

It should be stressed that the surface and chemical activity of melts in the UO_2–FeO_{1+x} system restrict the possibilities of using DTA for evaluating T_{liq} because of the melt interaction with the crucible material. In this case the IMCC method is preferable, because such interaction is eliminated. All the specimens for visual polythermal analysis (VPA) in a Galakhov microfurnace and DTA were prepared by quenching of the melt produced by the IMCC technique.

In order to get a sample having the eutectic composition, slow melt crystallization was carried out in the IMCC, which ensured the displacement of a eutectic liquid by the front of crystallization. As the more refractory materials crystallized out, the liquid composition became closer to the eutectic. The eutectic crystallization zone was recognized by the characteristic microstructure of the ingot.

In order to determine the solubility limit of FeO in the UO_2–FeO_{1+x} solid solution (SS) an additional experiment has been performed, in which UO_2–FeO_{1+x} SS was kept in long-term contact with a melt having a near-eutectic composition (≈1330 °C).

3. Results and discussion

Table 1 shows the composition of specimens produced by the induction melting using the cold-crucible (IMCC) method. The composition was determined by chemical and SEM/EDX analysis of the specimens' composition after the melt crystallization in the cold crucible. The table also gives eutectic and liquidus temperatures in the UO_2–FeO_{1+x} system determined by VPA IMCC, VPA in the Galakhov microfurnace and by DTA technique.

Table 1
Solidus and liquidus temperatures in the UO_2–FeO_{1+x} system[a]

UO_2 content (mol.%)	Temperature (°C)	
	Eutectic	Liquidus
3.9[a]	1332[c]	–
6.1[a]	–	1370[d]
6.2[a]	–	1463[c]
7.0[a]	1335[e]	–
9.4[a]	–	1593[c]
11.3[a]	–	1580[d]
14.0[a]	–	1518[c]
16.0[b]	–	1694[d]
21.4[b]	–	1802[d]
23.3[a]	–	1735[c]
23.5[a]	–	1815[d]
33.1[a]	–	2020[c]
33.9[b]	–	1959[d]
38.5[a]	–	2020[c]
43.5[a]	–	2050[c]
45.0	1335[e]	–
46.1[b]	–	2147[d]
67.5[b]	–	2368[d]

[a] – EDX results; [b] – chemical analysis results; [c] – visual polythermal analysis obtained in Galakhov microfurnace; [d] – visual polythermal analysis results obtained by IMCC; [e] – DTA results.

Based on the eutectic point in the UO_2–FeO_{1+x} system data, which resulted from thermodynamic calculations (Fig. 1) and experimental studies [7], the eutectic composition was found to be ≈3–5 mol.% UO_2. To refine these results a specimen having 3.9 mol % UO_2 was produced. The microstructure of the specimen section studied by SEM confirmed the eutectic character of the crystallization (Fig. 2(a)). According to the EDX analysis (Table 1) the average composition of this specimen corresponded to (4.0 ± 0.1) mol.% UO_2 (sample 1, SQ1, Table 2), which was in good agreement with the initial composition of the specimen and the data of [7], where the eutectic point corresponded to 3.3 mol.% UO_2.

Fig. 3 presents the thermogram of a specimen containing (7.0 ± 0.5) mol.% UO_2. The DTA heating curve (heating rate: 5 °C/min) exhibits two distinct endothermal effects with the onset at 1335 and 1379 °C. The former peak (with an asymmetric and broadened shape) seems to correspond first of all to eutectic melt formation in the system under

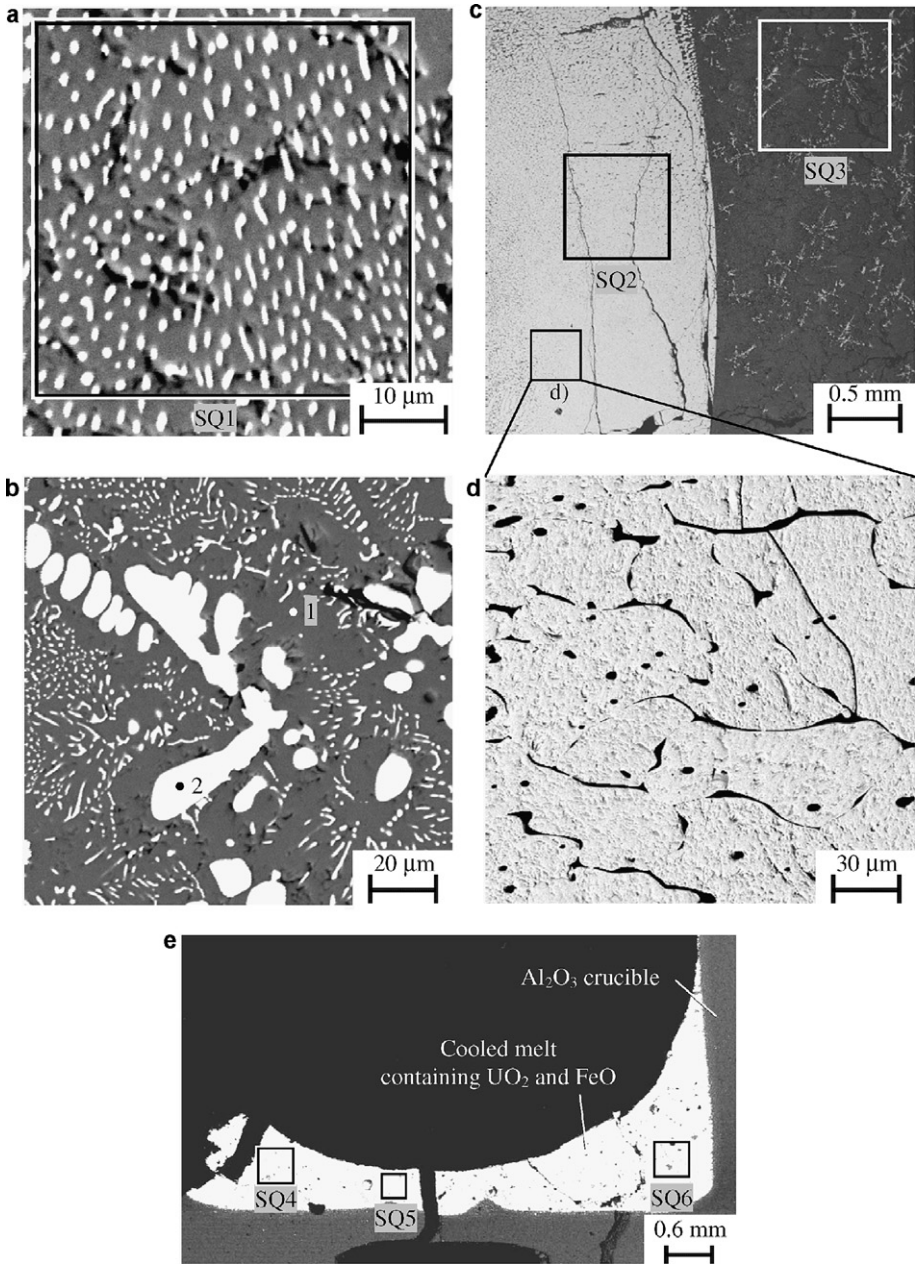

Fig. 2. Micrographs of the specimens crystallized in the UO_2–FeO_{1+x} system with different UO_2 contents: (a) 3.9 mol.% UO_2. (b) 7.0 mol.% UO_2, quenched after heating upto 1850 °C. (c) and (d) 21.0 mol.% UO_2 produced by the slow removal of ingot from the inductor. (e) 45.0 mol.% UO_2 after interaction with Al_2O_3 crucible.

investigation. At the first appearance of a liquid phase the activation of the interaction process between the UO_2–FeO_{1+x} system melt and the crucible material (Al_2O_3) takes place (Fig. 2(e)). This interaction is accompanied by Al_2O_3 dissolution in the UO_2–FeO_{1+x} eutectic melt. Therefore, the endothermal effect starting at 1379 °C should be attributed to the liquidus temperature of the UO_2–FeO–Al_2O_3 system. This consideration is confirmed by EDX analysis of the sample in the UO_2–FeO system after DTA (Fig. 2(e) and sample 4, Table 2). The cooling curve effects (Fig. 3) could be another circumstantial evidence of these results. The first exothermal effect started at 1393 °C (cooling rate:

Table 2
Chemical compositions of the areas marked in Fig. 2

Sample	UO_2 content (mol.%)	Examined areas	Composition of the phases (mol.%)		
			UO_2	FeO	Al_2O_3
1	3.9	SQ1	4.0	96.0	0
2	7.0	1	0	100	0
		2	95.5	4.5	0
3	21.0	SQ2	83.3	16.7	0
		SQ3	4.3	95.7	0
4	45.0	SQ4	37.12	57.04	5.84
		SQ5	38.16	56.07	5.77
		SQ6	16.72	68.67	14.61

5 °C/min) corresponding to the beginning of the melt crystallization is observed at a higher temperature because the melt was enriched with the refractory Al_2O_3 component. Therefore, as a reliable temperature in the UO_2–FeO_{1+x} system in this experiment we can consider only the eutectic temperature (1335 °C) because there were no interaction with the crucible material before a liquid phase appeared [11]. There appears to be little further interaction with the crucible during the crystallization as the offsets in temperatures for onset of melting on heating and completion of crystallization on cooling are similar to the offsets between completion of melting on heating and the onset of crystallization on cooling.

The phase corresponding to a UO_2-based SS has been found in practically all specimens (Fig. 2(b)). But the grains of the solid solution in most crystallized specimens were too small for the accurate determination of their composition by EDX; along with that, it has been noticed that UO_2–FeO_{1+x} SS decomposition on cooling forms a thick FeO layer (Fig. 2(b) and sample 2, point 1, Table 2) around urania-based grains (Fig. 2(b) and sample 2, point 2, Table 2). This can be probably explained by the reduction of the FeO solubility in the urania-based phase, as its temperature decreases. For these reasons an additional experiment was conducted, which was aimed at a more precise determination of final FeO solubility in UO_2. Using a start-up composition of 21.0 mol% UO_2 in the cold crucible, a layer of the UO_2–FeO_{1+x} SS was grown by a slow removal of the crucible from the inductor coil. A considerable thickness formed by the crystallization of the UO_2–FeO_{1+x} SS enabled more accurate data on the final solubility of FeO in UO_2 to be obtained. The SEM/EDX analysis of the UO_2-based SS (Fig. 2(c) and sample 3, SQ2, Table 2) has shown that besides the UO_2 phase a certain amount of a FeO-based phase was also presented (Fig. 2(d), dark domains in the light background). It could be explained by a partial decomposition of the UO_2–FeO SS during the specimen cooling, which was accompanied by the segregation of the FeO_{1+x} phase having the wüstite structure mainly located

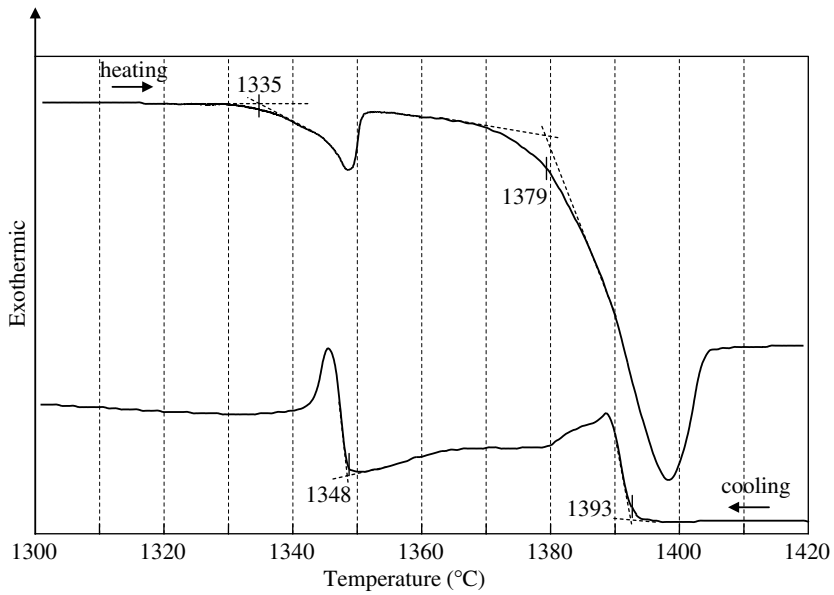

Fig. 3. DTA curve of the sample contained 7.0 mol.% UO_2 (inert atmosphere, corundum crucible), heating and cooling rate was 5 °C/min.

along the grain boundaries of this solid solution phase. The XRD pattern (Fig. 4) obtained with inner standard (Ge) allowed to estimate a unit cell parameter of the cubic UO_2-based SS too

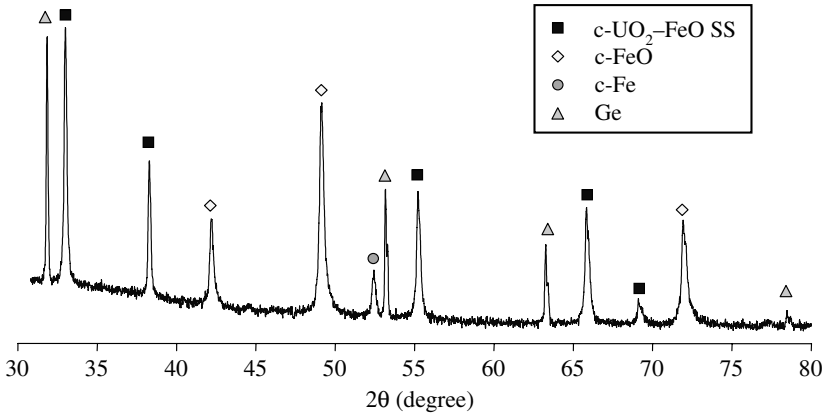

Fig. 4. X-ray diffraction pattern of the sample contained 3.9 mol.% UO_2, which has been kept in long-term equilibrium with the melt.

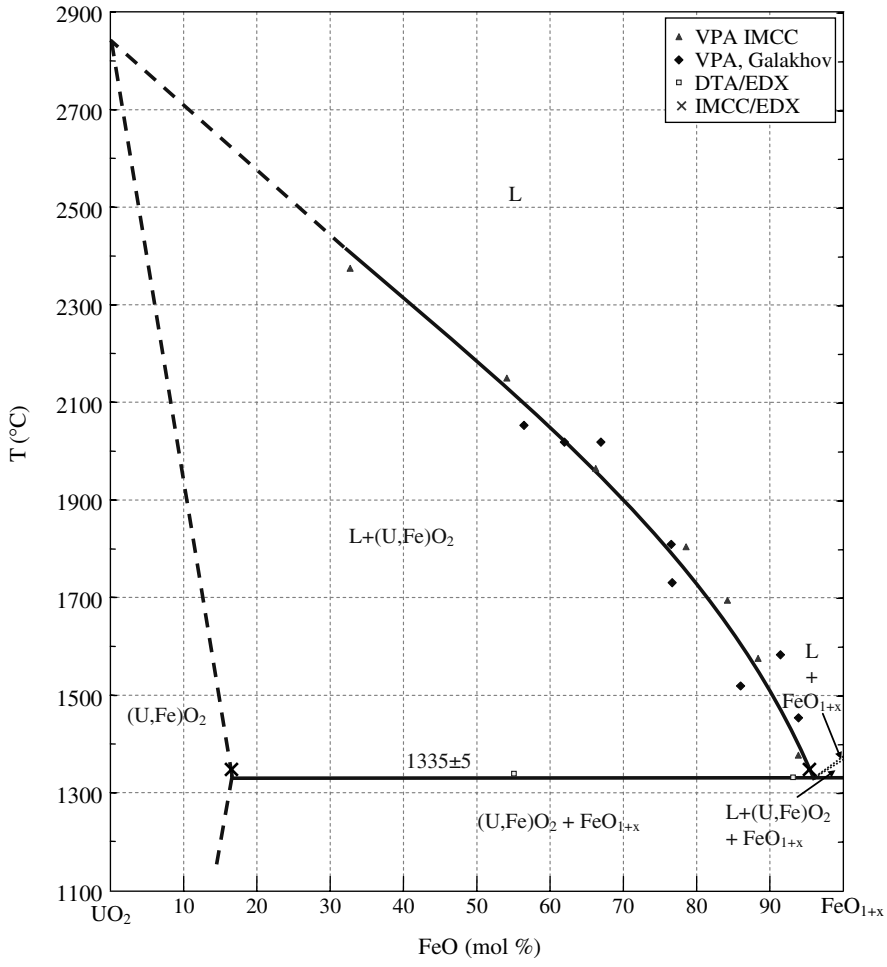

Fig. 5. Phase diagram of the UO_2–FeO_{1+x} system (inert atmosphere).

($a = (0.5442 \pm 0.0001)$ nm). The final $Fe_{1-\delta}O$ (FeO_{1+x}) composition in each case depends on a cooling rate of a sample and its composition (under the same p_{O_2} condition), as it can be concluded from the data given in the experimental work of Darken and Gurry [12] and is within the region of wüstite existence in the Fe–O phase diagram [10]. It should be noted here that the liquidus curve in the diagram was constructed under the conditions of Fe–FeO–UO_2 equilibrium.

The compositions of the studied specimens, the temperatures T_{eut} and T_{liq} evaluated by different methods (Tables 1 and 2), eutectic point composition, left hand liquidus curve and the maximum solubility of FeO in UO_2 have been used for the construction of a phase diagram of the UO_2–FeO_{1+x} system (Fig. 5).

The solid solution was found to coexist with the melt containing 4.3 mol.% UO_2 (Fig. 2(c) and sample 3, SQ3, Table 2) at the temperature of 1350 °C (Fig. 5). The FeO solubility in UO_2 determined by EDX was 16.7 mol.% (Fig. 2(c) and sample 3, SQ2, Table 2). The maximum solubility of FeO in UO_2 is known to be observed at the eutectic temperature. Therefore, extrapolating the solidus line through this point (1350 °C and 83.3 mol.% UO_2 – 16.7 mol.% FeO_{1+x}) downward down to the eutectic line (1335 °C) in the phase diagram (Fig. 5), yielded an estimated maximum solubility of FeO in UO_2 of $\approx(17.0 \pm 1.0)$ mol.% FeO.

It should be noted here that the SEM/EDX analysis did not detect the formation of the FeO-based SS in the system (Fig. 2 and sample 2, point 1, Table 2).

4. Conclusions

A phase diagram of the UO_2–FeO_{1+x} system has been constructed. It is a eutectic system with a region of the limited FeO solubility in UO_2. The eutectic composition and temperature of the system have been refined. The eutectic has a UO_2 content of (4.0 ± 0.1) mol.% and a temperature of (1335 ± 5) °C. The maximum solubility of FeO in UO_2 at the eutectic temperature is evaluated as (17.0 ± 1.0) mol.%, and a cell parameter of the cubic UO_2-based SS is estimated as $a = (0.5442 \pm 0.0001)$ nm.

The solidus and liquidus temperatures and specimen compositions determined by different methods have a good agreement within the measurement errors. This consistency demonstrates the reliability of the eutectic values presented here. These results are also able to refine the prior data points and thus improve the severe accident modelling of interactions of oxidic melts with vessel steel.

Acknowledgements

The work has been carried out within the ISTC CORPHAD project funded by the European Union. The authors express their gratitude to Dr A. Zurita, Professor L. Tocheny and Dr V. Rudneva for the coordination of the work on behalf of the European Commission and ISTC, and Dr Yu. Aniskevich for the project management. The authors highly appreciate useful comments and suggestions put forward by Dr G. Cognet and Dr B. Adroguer during the work planning and discussions at the annual project meetings.

References

[1] N.A. Toropov, V.P. Barzakovsky, V.V. Lapin, N.N. Kurtseva, Phase diagrams of silicate systems, Russ. Reference bookBinary systems, vol. 1, Nauka, Moscow–Leningrad, 1965.
[2] V.V. Gusarov, V.I. Al'myashev, S.V. Beshta, V.B. Khabenskii, Yu.P. Udalov, V.S. Granovskii, Therm. Eng. 48 (2001) 721.
[3] Russian Federation Patent No. 2192053, Oxidic material of the core catcher, Application 12001128174/06, date of publication: 27.10.2002. Priority of 12.10.2001, V.V. Gusarov, V.I. Almiashev, V.L. Stoliarova et al.
[4] V.V. Gusarov, V.B. Khabensky, S.V. Beshta et al., China Patent ZL 02807587.0, date of publication, July 13, 2005. Priority of 02.04.2002.
[5] M. Fischer, Nucl. Eng. Des. 230 (2004) 169.
[6] L.F. Epstein, W.H. Howland, J. Am. Ceram. Soc. 36 (1953) 334.
[7] S. Hellmann, F. Funke, M. Fischer, D.B. Lopukh, S.V. Beshta, New experiments on the interaction of ZrO_2 material with corium melts and phase diagram points in UO_2-based systems. CIT Project Report, Corium Interactions and Thermochemistry, In-Vessel Cluster, INV – CIT(99)-P037, December 1999.
[8] N.M. Voronov, R.M. Sofronova, V.A. Voytekhova, High-temperature chemistry of uranium oxides and their compounds, Atomizdat, Moscow, 1971, (in Russian).
[9] S.V. Bechta, E.V. Krushinov, V.I. Almyashev, et al., J. Nucl. Mater. 348 (2006) 114.
[10] H.A. Wriedt, J. Phase Equilib. 12 (1991) 170.
[11] V.V. Gusarov, Russ. J. General Chem. 67 (1997) 1846.
[12] L.S. Darken, R.W. Gurry, J. Am. Chem. Soc. 67 (1945) 1398.